Sensor and Simulation Notes

Note 583

June 2020

Multiband and Tunable HPM Radiator Combining Frequency Selective Surfaces with a Hyperband Source
Part I – Theoretical analysis

Fernando Albarracin-Vargas[1], Felix Vega[1,2], Chaouki Kasmi[1,3],
David Martinez[1], Fahad Alyafei[1], Lars Ole Fichte[3]

[1]Directed Energy Research Centre, TII, Abu Dhabi, United Arab Emirates
[2]Universidad Nacional de Colombia - Sede Bogotá, Bogotá, Colombia,
[3]Faculty of Electrical Engineering, Helmut Schmidt University,
Hamburg, Germany.
Email: fernando.albarracin@derc.tii.ae

Abstract

This paper presents a new contribution to a resonant radiator, obtained as a combination of a Frequency Selective Surface (FSS) and an Impulse Radiating Antenna (IRA). The effects of a multiband FSS are studied and verified via simulations. A multiband radiator is obtained, enabling the capability of modifying the emitted signal for multiple applications, like EMI testing, or the development of hardening modules to be integrated into facilities. Two different approaches are presented. First, a dual-band FSS is integrated into the IRA to verify the filtering effect in the radiated pulse. Second, a multilayer FSS is utilized as a tunable narrowband filter for the IRA. The frequency agility of the radiator is proposed to be implemented via a piezoelectric actuator.

1. INTRODUCTION

The radiation of fast transient electromagnetic pulses produced by High Power Microwave (HPM) sources, is a topic of interest for the academic community and defense industry. It is related to the potential disruption of electrical systems and high technology microcircuits, both part of the critical infrastructure of a country. The characterization of such disruptions is subject of Intentional Electromagnetic Interference (IEMI) and Compatibility (EMC) studies [1], [2]. A key part of the design of a pulse radiator is the antenna system. This involves the use of radiators with the ability to radiate at low frequency, nearly constant gain and impedance over bandwidth ratios greater than 10 (i.e., hyperband region), and high-voltage handling capabilities. The Impulse Radiating Antenna (IRA), first proposed by Baum and Farr [3]–[5], is one of the most representative types of hyperband radiators for IEMI tests, due to its hyper-band response and high-voltage capability. The working principle of an IRA is to launch a spherical and non-dispersive TEM wave-front from the focal point of a parabolic reflector. Such a TEM spherical wave propagates through the feeder arms, that act as a TEM transmission line.

Both components mentioned so far, the antenna and the pulsed source, share two important characteristics: high cost and fixed working bandwidth. In this context, the use of a frequency selective planar structure arises as a strategy to add frequency agility to the complete system Antenna+HPM source. The ability to radiate over multiple bands is possible by arranging multiple resonating unit-cell types into the Frequency Selective Surface (FSS), or by changing the separation of a multilayer lattice.

In related studies, it has been shown that a metal-grid embedded within the walls of a building displays interesting properties when illuminated with an ultra-wideband (UWB) radiator. Tesche et al. [6] analyzed the possibility of damping the emitted pulse signal by chaining a set of metal grids placed in front of the antenna. These serve to transform the fast-pseudo-impulse from the antenna into a damped sinusoidal waveform. The attenuation effect, due to reinforced concrete walls, in the downlink bands of mobile communication systems, is studied in [7]. A low-pass FSS that can be integrated into an ultra-wideband radiator was presented in [8]. Other alternatives, like the use of self-actuated surfaces, using arrays of semiconductors, are described in [9], [10]. Voltage-controlled piezoelectric actuators are used to tune an FSS in [11].

FSSs are narrowband passive structures that exhibit interesting properties when illuminated by electromagnetic fields. In their more usual form, FSSs are implemented as resonant metal elements, or apertures, electrically small compared to its resonance frequency, placed periodically over a containing surface or substrate [12]. The well-known Split Ring Resonators (SRR) proposed in [13], and its complementary version (i.e., CSRR), have been studied and characterized in the last years as a compact structure to compose an FSS [12], [14]. To avoid diffractive effects and grating-lobes on the intended radiated beam, both the unit cell size and separation must be smaller than the wavelength of the incident radiation.

A relevant characteristic of these resonators is the capability of being cross-polarized. In an SRR, a polarizing surface results by either the E- or the H-field passing through the structure. This phenomenon produces a band-stop response [12]. On the other hand, an electric dipole is induced from the excitation of a CSRR with an incident wave whose electric field component is parallel to the rings' gaps, resulting in a bandpass filtering surface. Marques et al. [12] presented an analytical solution for the behavior of FSS based on SRR and CSRR cells. Although restricted to the infinitesimally thin perfect conductor in free space, the analytical approach gives a first approximation to the response of a band-pass-type FSS.

This work presents an alternative to the design of integrated multiband and tunable HPM radiators, composed of a CSRR-based FSS in the near-field of a hyperband radiator, like the IRA. All the designs presented comprise a strategy to add waveform and frequency agility to the resulting HPM source: IRA+FSS. Three different approaches to the FSS are proposed—first, a single-narrowband FSS composed of coplanar CSRR placed in a single layer. Second, a multiband FSS with the ability to radiate over multiple bands by arranging multiple-size resonating unit-cell into a single layer FSS. Finally, a tunable FSS based on a broadside-coupled complementary ring resonator. The tunability approach involves the use of piezoelectric actuators that modify the separation between the layers of the FSS. The tunable integrated HPM source approach and the unit cell designs are described in Section II. The cascaded-system analysis of the integrated radiator is presented in Section III. Results and conclusions are included in Section IV and Section V, respectively.

2. TUNABLE HPM SOURCE APPROACH

The multiband radiator proposed here is depicted in Figure 1. The FSS acts as a passband filter with a high Q-factor response. The FSS is acting as a bandpass filter, modifying the impulse-like waveform radiated from the IRA by converting it into a damped sinusoid, with one or multiple frequency components. Only the electric field components aligned with the CSRR gaps, and around the resonant frequency of each unit cell, will effectively pass through the FSS [12]. Unit cells of the same size are aligned along the vertical *y*-axis to align each resonant polarization with the incoming wideband transient wave from the hyperband radiator.

The spectral content of the radiated field of the resultant HPM radiator depends on the frequency agility of the FSS. Three different types of bandpass FSS are presented in the next sections.
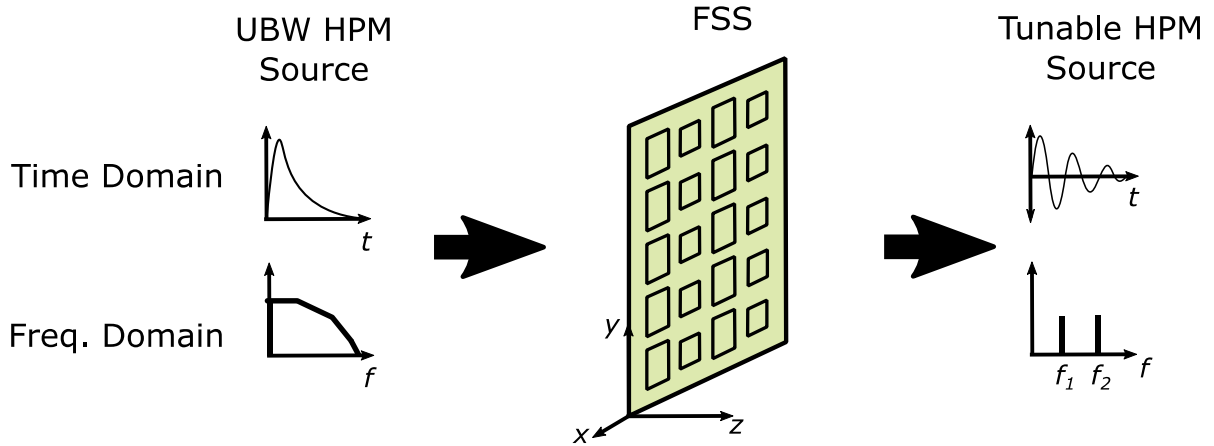
Figure 1. Multiband HMP Radiator scenario

2.1. SINGLE BANDPASS FSS DESIGN

Since the baseline is to retrieve a narrowband signal (ideally a single frequency) after the signal from the IRA passes through the FSS, a high Q-factor unit cell should be used. As mentioned above, we have designed a Complementary Split Ring Resonator (CSRR) first proposed in [14], as the one depicted in Figure 2a. The transmission and reflection parameters of the simulated CSRR-based FSS are shown in Figure 2b. It can be seen the narrowband response of the FSS, and its suitability to be used as a high-Q bandpass filter. The unit cell has been simulated as an infinite periodic structure. The 3dB-bandwidth of the pass band around $f_0 = 1.49$ GHz is 35 MHz (2.33%). The Q-factor, $Q = f_0/BW_{-3dB}$, yields 42.8.

(a)

(b)
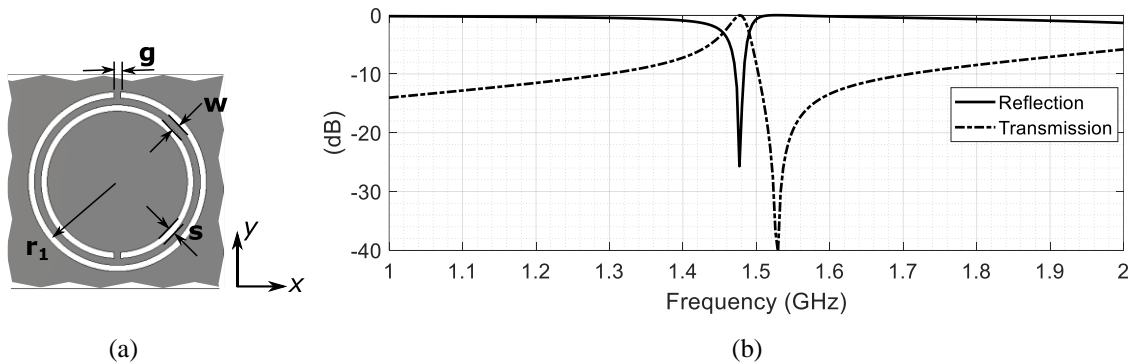
Figure 2. (a) Geometry of the CSRR (unit-cell). w =3.9; r_1 = 13.3; g =1; s = 1.1. All the dimensions are in mm. The substrate (white colored background between the rings) is 1 mm thick, with ε_r = 1. (b) Simulated transmission and reflection parameters of the CSRR-based FSS.

2.2. MULTIBAND FSS: UNIT CELL DESIGN

The proposed unit cell is composed of two different CSRRs configured as depicted in Figure 3a. Since the intended response of the FSS is multiband, each band shall be tuned according to the resonant frequency of each unit-cell size. Only waves whose electric field is aligned to the gaps in the rings (*y*-axis in Figure 3a) will be able to pass through the FSS, at frequencies slightly higher than the resonant

frequencies of the composing CSRR cells. Figure 3b shows the scattering parameters for the multiband FSS. An additional resonant frequency is observed at 2.6 GHz. This response is associated with a higher frequency resonance of the 1.5 GHz unit cell.
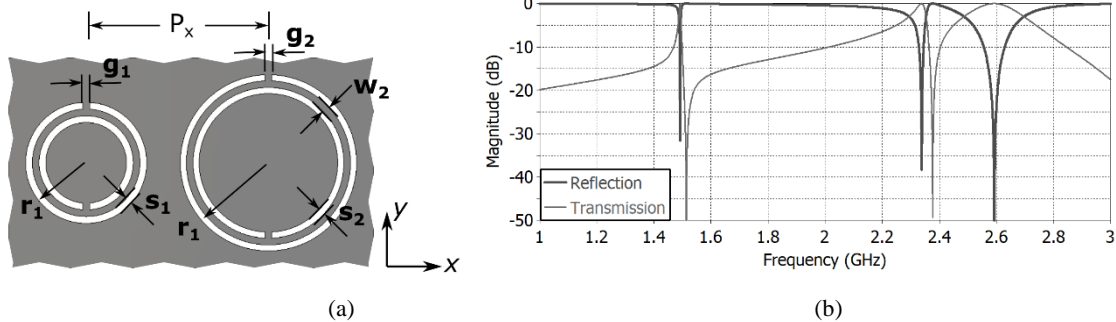
Figure 3. (a) Sketch of the dual-band CSRR unit cell geometry. Unit cell 1, on the left, is associated with a passband frequency of around 2.4 GHz. The unit cell on the right is resonant at 1.5 GHz. The dimensions are (all in mm) P_x= 26.5, P_y= 26.5, r_1=8.5, r_2=12.65, g_1=g_2=1, s_1= s_2=1, w_1=w_2=1. (b) FSS response in frequency, simulated as an infinite periodic structure.

The 3dB-bandwidth calculated around the 1.5 GHz band is 10 MHz (0.66%), which corresponds to a Q-factor of 150. For the 2.4 GHz band, the 3-dB bandwidth is 56 MHz (2.33%), with a Q-factor of 42.8.

2.3. BROADSIDE COUPLED TUNABLE FSS

A modified version of the CSRR is now used as its broadside configuration (see Figure 4 as a reference), to implement a bandpass FSS. By modifying the separation between the conductive layers, the pass band is tuned. The study of the frequency agility considers the typical displacement from off-the-shelf piezoelectric actuators [11]. The proposed CSRR composing the FSS comprises two conductive layers, separated by a low permittivity substrate, (ideally ε_r = 1), of variable width, simulated as loss-free for a first approximation. Each cell contains a ring-shaped slot with a gap, broadside coupled, located at each face of the double-sided substrate slab, as shown in Figure 4. In this configuration, the gaps of the unit cell (g_1 and g_2 in Figure 4) are located diametrically opposed to each other. Thus, the two layers of the FSS are identical in shape but turned 180 degrees one with respect to the other. The FSS resonates at 1.87 GHz for the minimum ring separation. The separation between rings ranges from 1.2 mm to 2 mm (i.e., Δh = 0.8 mm).
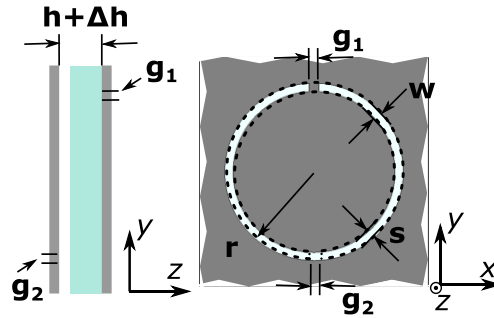
Figure 4. Broadside-coupled CSRR unit cell. The dimensions are (all in mm): r = 8.3, g_1 = g_2 = 1, s= 1, w= 1. g_1 is in the top layer while g_2 is in the bottom (slotted line) layer. The dielectric thickness, $h = 1.2 + \Delta h$, is the tuning parameter. Δh ranges from 0 to 0.8 mm. Conductor thickness is 0.05 mm.

The frequency response of the FSS is shown in Figure 5. The pass band shows a -3dB bandwidth of 120 MHz (6%) for all the ring separations. The complete tunability range is around 310 MHz for a substrate width, $h+\Delta h$, from 1.2 to 2.0 mm.

(a)

(b)
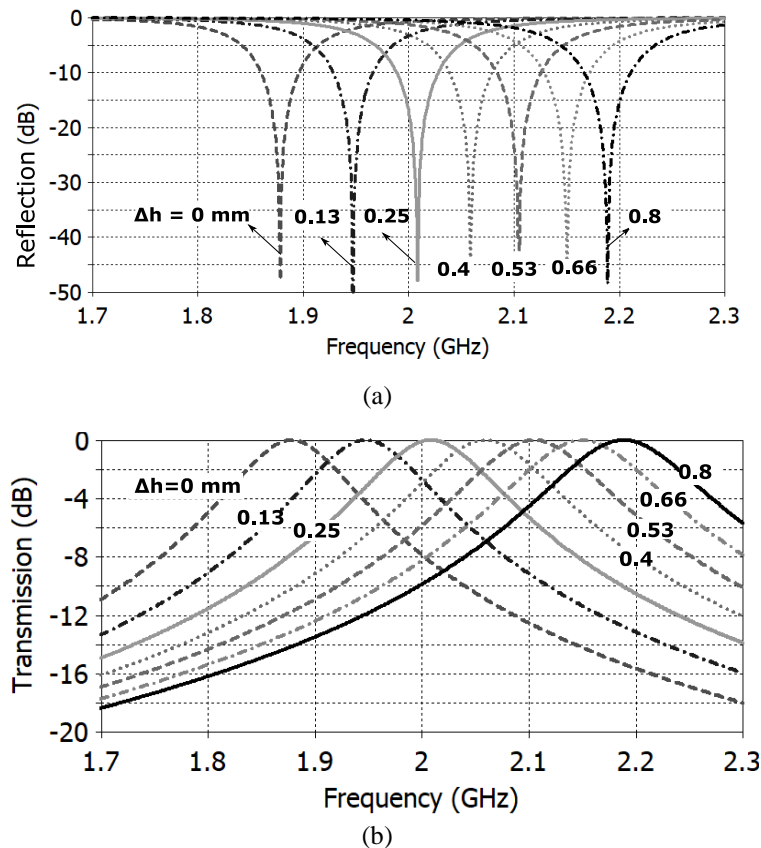
Figure 5. Broadside coupled FSS simulated as an infinite periodic structure. (a) Reflection, and (b) transmission parameter.

3. INTEGRATED RADIATOR

3.1. REFLECTOR BASED IRA

The sketch of a two-arm IRA is shown in Figure 6. When connected to a pulsed voltage source, the IRA radiates an impulse-like waveform over a narrow beam in the boresight direction (z-axis in Figure 6). The electric field related to the waveform radiated by the IRA can be described as [15]:

$$E_t(t,r) = f_1 \frac{1}{2\pi f_g} \left(\frac{\frac{V(t-r/c)}{r} \frac{\sin(\beta)}{1+\cos(\beta)} - \frac{V(t-l/c-R_2/c)}{R_2} \frac{\sin(\beta)+\sin(\gamma)}{1+\cos(\beta-\gamma)} \cdots}{-\frac{4}{D}V(t-2F/c-r/c)+(2+2\cos(\gamma))\frac{V(t-l/c-R_2/c)}{D}} \right) \left(\frac{V}{m} \right) \tag{1}$$

where $V(t)$ is the feeding voltage, $f_1 = 1$ for the two-arm IRA, c is the speed of light, and r is the distance between the focal point and the measurement point. The geometric impedance factor, $f_g = Z_{IRA}/120\pi$, is a reference parameter related to the feeder geometry that transmits the spherical TEM wave into the reflector. Z_{IRA} is the input impedance of the antenna. $D, F, l, \beta, \gamma,$ and R_2 are described in Figure 6. The two-arm IRA presented in this paper is designed with the following parameters: $D = 1(m)$, $F/D = 0.4$, $Z_{IRA} = 400 (\Omega)$.
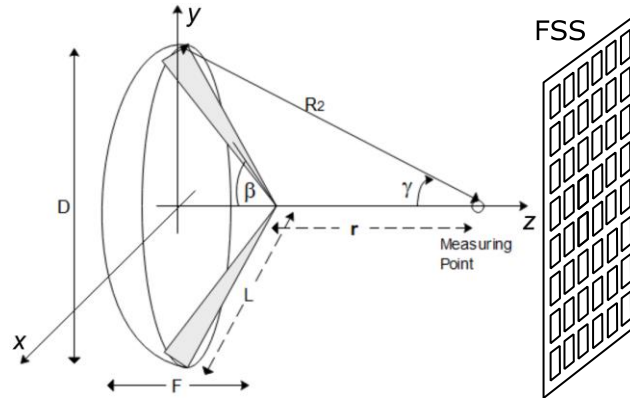
Figure 6. IRA geometry integrated with an FSS composed of the CSRR unit cell. The actual distance between the IRA and the FSS is shorter than sketched.

3.2. CASCADED SYSTEM ANALYSIS

The field radiated from the IRA in Equation (1) can be related to the voltage at the feed point through the transfer function, $T_A(f)$, computed as

$$T_A(f) = E_{IRA}(f)/V_{in}(f) \tag{2}$$

Note that the $E_{IRA}(f)$ does not necessarily have to be computed in the far-field region. Due to the nature of the radiation from a parabolic reflector, a normally incident EM field propagates through the FSS from the left (see Figure 6), and continues along the z-axis, but with its spectral characteristics filtered. By applying the *chain parameters approach* [6], it is possible to represent the FSS by a linear two-port circuit. The conventional currents and voltages are linearly related to the tangential components of the E- and H-fields at the input and output ports, as depicted in Figure 7. This yields to

$$\begin{bmatrix} E_{1,\tan} \\ H_{1,\tan} \end{bmatrix} = \begin{bmatrix} A & B \\ C & D \end{bmatrix} \begin{bmatrix} E_{2,\tan} \\ H_{2,\tan} \end{bmatrix} \tag{3}$$

Then, the transfer function of the FSS can be easily computed from its scattering parameters, like those shown in Figure 3 and Figure 5 for the multiband and the broadside-tunable cell, respectively. In this model, $E_{1,tan}(f) = E_{IRA}(f)$. The tangential output field, $E_{IRA+FSS}(f)$ in the y-axis direction, can be computed as

$$E_{IRA+FSS} = E_{2,\tan} = 2E_{1,\tan} \left(\frac{\eta_0}{\eta_0(\eta_0 A + C) + (B + \eta_0 D)} \right) \tag{4}$$

$$E_{IRA+FSS} \equiv T_{FSS}(f)E_{1,\tan}(f)$$

where η_0 is the free space impedance (i.e., 377 Ω).
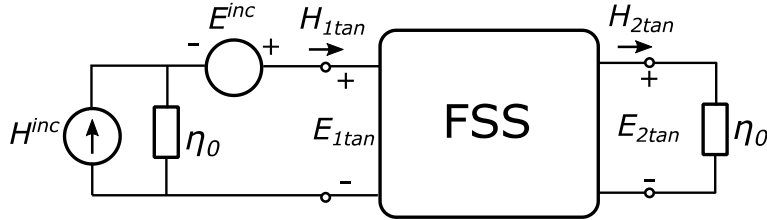
Figure 7. FSS, as an ABCD parameter circuit representation [6]. Tangential E- and H-field replace voltage and current of a conventional model.

Finally, an expression for the electric field once the transient pulse passes through the FSS is as follows

$$T_{Total}(f) = T_A(f) \cdot T_{FSS}(f) \tag{5}$$

$$E_{IRA+FSS}(f) = T_{Total}(f) \cdot V_{in}(f) \tag{6}$$

Once the complete transfer function of the integrated IRA+FSS radiator is extracted, the spectral response of the electric field waveform, related to a pulsed voltage signal driving the IRA terminals, i.e.,

$V_{in}(f)$, can be analytically evaluated, as it will be shown below. The electric field in the time domain can be computed as the inverse Fourier transform of $E_{IRA+FSS}(f)$.

4. RESULTS

The integrated FSS+IRA radiator is modeled in a commercial full-wave simulator. A square array of unit cells is designed to cover 1 m^2, which is the area circumscribing the reflector aperture. In both FSS topologies we are illustrating, the FSS structure is located 10 cm away from the focal point of the IRA. Although a larger separation between FSS and antenna would minimize multiple reflections, diffracted waves from the perimeter of the FSS structure will have a more significant effect in the filtered pulse.

The multiband FSS is designed by arranging 22 X 36 unit cells (see Figure 3a for a reference). The whole system, IRA+FSS, is gridded into a 50 million cell mesh, applying a symmetry around the xz-plane (see Figure 6). The simulation time reached 2 hours in a computer with a GPU of 512 cores and 6 GB memory size. The electric field has been computed 5 m away from the focal point of the IRA, in broadside (z-axis). The time-domain response of the radiated electric field is shown in Figure 8a. The field radiated by a conventional two-arm unloaded IRA, with the same dimensions, is also shown as a reference. In both cases, a Gaussian pulse, with spectral content ranging from 0 to 3.5 GHz and 18 V in amplitude, is used as the driving signal. The damped-like sinusoidal response of the proposed design is observed, as expected.

The passband filtering behavior of the FSS loading the IRA is observed in the frequency domain response of the electric field, as shown in Figure 8b. The ideal filtering response of the IRA+FSS system can also be computed by applying the chain parameter analysis described by equations (2)-(6), and is shown as a reference. For the ideal system response, the ABCD parameters of the FSS have been computed from the single unit cell simulation, using the infinite periodic boundary conditions capability of the simulator. This leads to a significantly shorted simulation time since the IRA is simulated apart from the FSS.

Despite the amplitude drop in the full-wave simulated IRA+FSS field, the intended passband effect holds around the resonant frequency of each unit-cell size, as can be seen in Figure 8b. Ideally, the impulse-like radiated pulse shall be converted into a signal with two different frequency components. However, harmonic resonances from the unit cells limit the bandwidth operation of the integrated radiator, as observed in the overlapped band around 2.6 GHz.
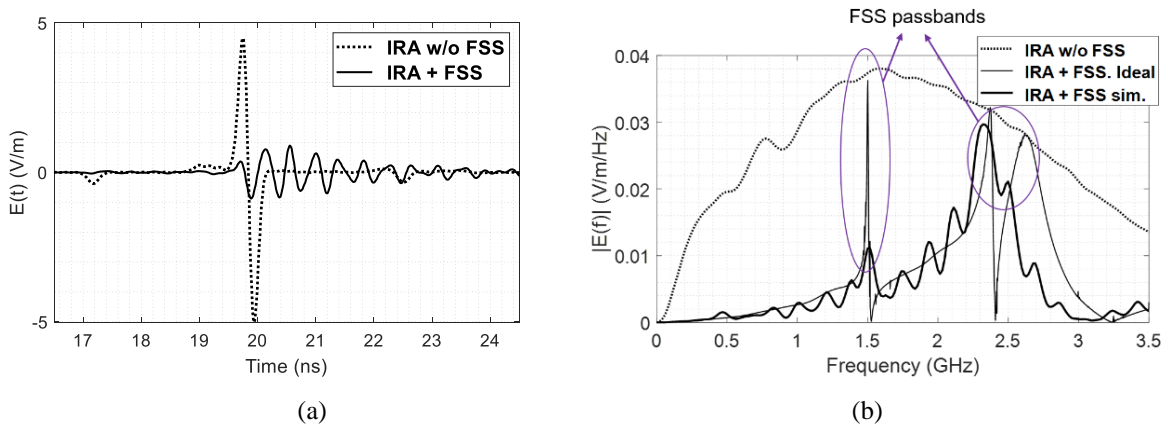
Figure 8. IRA vs. IRA+FSS: (a) time-domain and (b) spectral magnitude response in farfield, on boresight.

Since the proposed multiband FSS presents bilateral symmetry over the main planes around the axis of the reflector, i.e., *xz*-plane and *yz*-plane in Figure 6, symmetric and still directive radiation pattern can be expected, as it is shown in Figure 9. A significant degradation in the SLL ratio is observed in both frequency bands, especially in the E-plane. This can be associated with the limited size of the FSS (approximately 1 x 1 m^2) that was finally integrated into the radiator. The effects of diffraction due to the FSS edge are evident. At higher frequencies (e.g., 2.4 GHz), this phenomenon is less prominent but still significant. One possible solution for this problem can be simply increasing the total area of the FSS, at the expense of affecting the manageability of the radiator. The maximum directivity is decreased from 18 dBi to 11 dBi at 1.5 GHz, while remained 22 dBi at 2.4 GHz. This response is in accordance with the higher field strength around 2.4 GHz once the wave passes through the FSS (see Figure 8b).
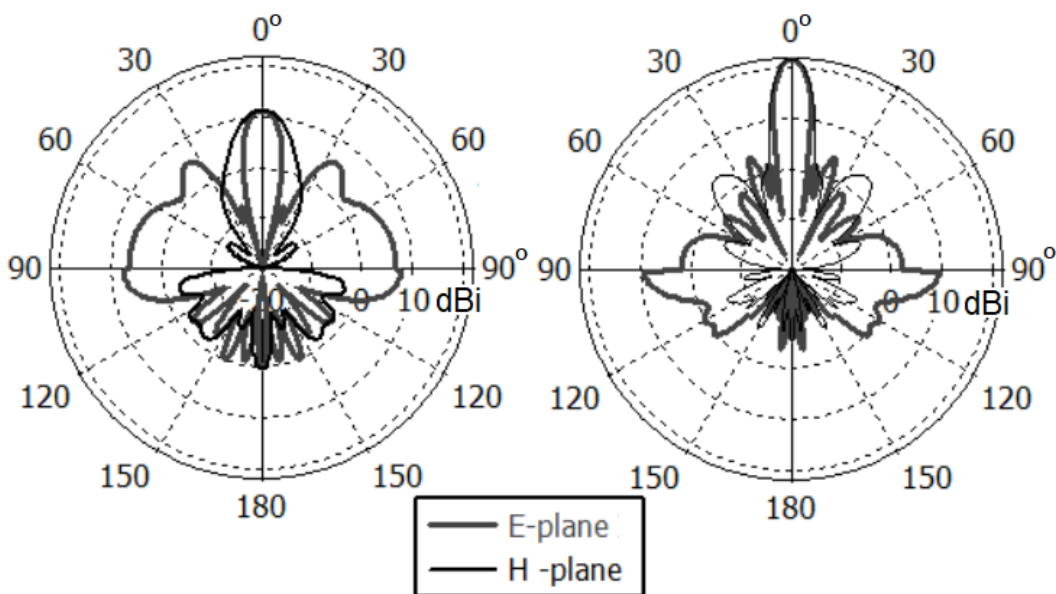
Figure 9. Radiation response of the integrated radiator, IRA+FSS at (a) 1.5 GHz, and (b) 2.4 GHz.

For the case of the broadside-coupled tunable FSS-IRA radiator, the tunable response of the unit cell is computed as a parametric analysis for different separation values, Δh, ranging from 0 to 0.8 mm. Figure 10 presents the spectral amplitude of the electric field, 5 m away from the focal point. The cascaded system approach is utilized for this analysis. It is observed the expected filtering effect of the FSS on the spectral response, as compared to the reference IRA. The antenna is fed with a Gaussian pulse of 18 V in amplitude.
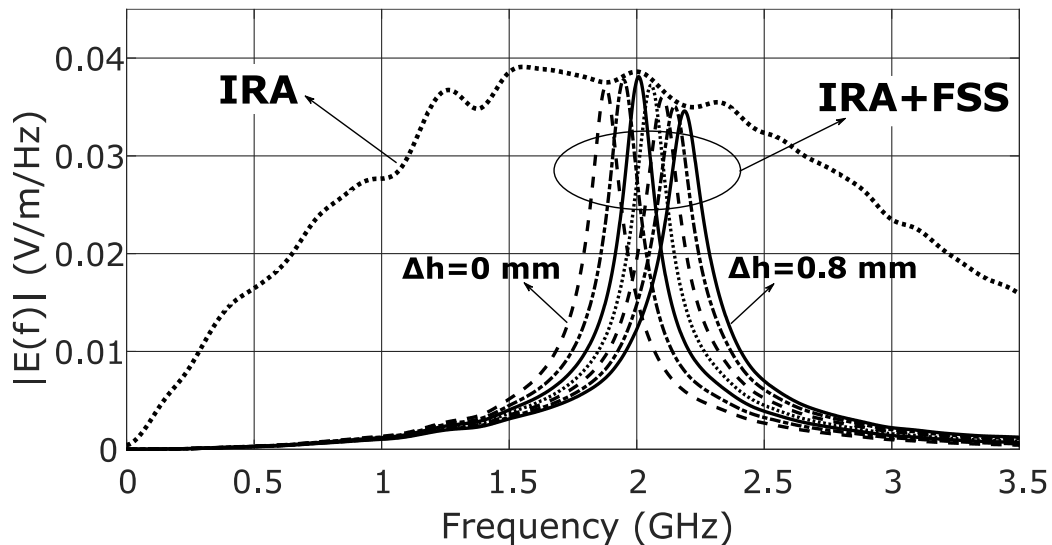
Figure 10. The spectral magnitude of the electric field radiated by the integrated IRA+FSS radiator. The FSS acts as a tunable high-Q passband filter. The field radiated by the unloaded IRA is shown as a reference.

The frequency agility of the tunable FSS ranges from 1.7 GHz to 2.3 GHz, which represents 25 % of fractional bandwidth. This characteristic can be improved by using piezoelectric actuators with higher effective displacements or by implementing other mechanical alternatives to control the ring separation.

5. CONCLUSION

The design of a narrowband HPM radiator by the integration of a high-Q bandpass FSS with a hyperband radiator is presented. The analytical and numerical responses of the radiated field have been described and verified via full-wave simulations. A high-Q FSS implemented with CSRR cells is an attractive alternative for effectively modifying the radiated waveform from a UWB radiator. These can be suitable for different IEMI test scenarios, using one single UWB radiator.

Different configurations for the FSS have been proposed and analyzed. The multiband FSS permits a dual-band damped signal whose pass bands are a function of the cell geometry. However, the harmonic resonances at higher frequencies limit the spectral separation to less than one octave above the first resonant cell.

On the other hand, the broadside-coupled tunable IRA-FSS radiator presents an important advantage by its 25% tunability with a 6% in instantaneous bandwidth. This characteristic enables the capacity of conducting susceptibility tests in multichannel systems under a wider variety of conditions.

Future work will be dedicated to implement a prototype to verify the design is under way and will be presented in a future part II manuscript.

REFERENCES

[1] D. Shyamala, R. Kichouliya, P. Kumar, S. Satav, and R. Dasari, "Experimental Studies and Analysis on IEMI Source, Field Propagation and IEMI Coupling to Power Utility System," *Progress In Electromagnetics Research*, vol. 83, pp. 229–244, 2018, doi: 10.2528/PIERC17111706.

[2] C. E. Baum, E. G. Farr, and D. V. Giri, "Review of impulse-radiating antennas," *Review of Radio Science*, pp. 403–439, 1999.

[3] C. E. Baum, "Radiation of Impulse-Like Transient Fields," *Sensor and Simulation Notes 321*, p. 28, Nov. 1989.

[4] C. E. Baum and E. G. Farr, "Impulse Radiating Antennas," in *Ultra-Wideband, Short-Pulse Electromagnetics 2*, H. L. Bertoni, L. Carin, and L. B. Felsen, Eds. Boston, MA: Springer US, 1993, pp. 139–147.

[5] C. E. Baum, "Aperture Efficiencies for IRAs," *Sensor and Simulation Notes*, no. 328, Jun. 1991, [Online]. Available: http://ece-research.unm.edu/summa/notes/SSN/note328.pdf.

[6] F. M. Tesche and D. V. Giri, "Modification of Impulse-Radiating Antenna Waveforms for Infrastructure Element Testing," *Sensor and Simulation Notes*, vol. 572, p. 25.

[7] G. Antonini, A. Orlandi, and S. D'elia, "Shielding effects of reinforced concrete structures to electromagnetic fields due to GSM and UMTS systems," *IEEE Transactions on Magnetics*, vol. 39, no. 3, pp. 1582–1585, May 2003, doi: 10.1109/TMAG.2003.810327.

[8] W. Bigelow, E. G. Farr, and J. S. Tyo, "A Frequency Selective Surface Used as a Broadband Filter to Pass Low-Frequency UWB while Reflecting X–Band Radar," *Sensor and Simulation Notes*, no. 506, 2006, [Online]. Available: http://ece-research.unm.edu/summa/notes/SSN/Note506.pdf.

[9] C. Yang, P.-G. Liu, and X.-J. Huang, "A Novel Method of Energy Selective Surface for Adaptive HPM/EMP Protection," *IEEE Antennas and Wireless Propagation Letters*, vol. 12, pp. 112–115, 2013, doi: 10.1109/LAWP.2013.2243105.

[10] S. Monni *et al.*, "Limiting frequency selective surfaces," in *2009 European Microwave Conference (EuMC)*, Sep. 2009, pp. 606–609, doi: 10.23919/EUMC.2009.5296360.

[11] M. Mavridou, K. Konstantinidis, A. Feresidis, and P. Gardner, "Novel tunable frequency selective meta-surfaces," in *2016 46th European Microwave Conference (EuMC)*, Oct. 2016, pp. 301–304, doi: 10.1109/EuMC.2016.7824338.

[12] R. Marques *et al.*, "Ab initio analysis of frequency selective surfaces based on conventional and complementary split ring resonators," 2005, doi: 10.1088/1464-4258/7/2/005.

[13] J. B. Pendry, A. J. Holden, D. J. Robbins, and W. J. Stewart, "Magnetism from conductors and enhanced nonlinear phenomena," *IEEE Transactions on Microwave Theory and Techniques*, vol. 47, no. 11, pp. 2075–2084, Nov. 1999, doi: 10.1109/22.798002.

[14] J. D. Ortiz, J. D. Baena, V. Losada, F. Medina, and J. L. Araque, "Spatial Angular Filtering by FSSs Made of Chains of Interconnected SRRs and CSRRs," *IEEE Microwave and Wireless Components Letters*, vol. 23, no. 9, pp. 477–479, Sep. 2013, doi: 10.1109/LMWC.2013.2274997.

[15] O. V. Mikheev, S. A. Podosenov, K. Y. Sakharov, A. A. Sokolov, Y. G. Svekis, and V. A. Turkin, "New method for calculating pulse radiation from an antenna with a reflector," *IEEE Transactions on Electromagnetic Compatibility*, vol. 39, no. 1, pp. 48–54, Feb. 1997, doi: 10.1109/15.554694.